



Cite this: *RSC Adv.*, 2023, **13**, 15960

Mussel-inspired polydopamine decorated silane modified-electroconductive gelatin-PEDOT:PSS scaffolds for bone regeneration

Catalina Adler,^{ab} Mahshid Monavari,^b Gustavo A. Abraham,^{ac} Aldo R. Boccaccini  ^{*b} and Farnaz Ghorbani  ^{*b}

This study seeks to simulate both the chemistry and piezoelectricity of bone by synthesizing electroconductive silane-modified gelatin-poly(3,4-ethylenedioxythiophene) polystyrene sulfonate (PEDOT:PSS) scaffolds using the freeze drying technique. In order to enhance hydrophilicity, cell interaction, and biomineralization, the scaffolds were functionalized with polydopamine (PDA) inspired by mussels. Physicochemical, electrical, and mechanical analyses were conducted on the scaffolds, as well as *in vitro* evaluations using the osteosarcoma cell line MG-63. It was found that scaffolds had interconnected porous structures, so the PDA layer formation reduced the size of pores while maintaining scaffold uniformity. PDA functionalization reduced the electrical resistance of the constructs while improving their hydrophilicity, compressive strength, and modulus. As a result of the PDA functionalization and the use of silane coupling agents, higher stability and durability were achieved as well as an improvement in biomineralization capability after being soaked in SBF solution for a month. Additionally, the PDA coating enabled the constructs to enhance viability, adhesion, and proliferation of MG-63 cells, as well as to express alkaline phosphatase and deposit HA, indicating that scaffolds can be used for bone regeneration. Therefore, the PDA-coated scaffolds developed in this study and the non-toxic performance of PEDOT:PSS present a promising approach for further *in vitro* and *in vivo* studies.

Received 26th February 2023

Accepted 15th May 2023

DOI: 10.1039/d3ra01311a

rsc.li/rsc-advances

1. Introduction

As a result of trauma or disease, bone loss is becoming an increasingly prevalent health issue. Therefore, bone must be regenerated in order to fill in a defect and restore structural and functional integrity to the tissue. In spite of the fact that bone has a self-healing capacity,¹ large defects will require external interventions in order to regenerate effectively. In order to achieve appropriate healing, an effective strategy must be found considering the complex structure and performance of bone tissue. While some therapeutic substrates have shown promising results, there are a number of drawbacks (poor restoration of biochemical and biomechanical function, lack of porosity, unsuitable durability of products as well as loosening and toxic byproducts with pH changes causing inflammation, *etc.*) that prevent satisfactory results in the repair of large bone defects.^{2,3} For this issue, tissue engineering (TE) represents a favorable

approach that combines the body's natural biological responses with engineering approaches to regenerate damaged tissues.⁴ In addition to providing physical support for cells, TE scaffolds must also act as a substrate for cell proliferation, migration, differentiation, and secretion of extracellular matrix (ECM).⁵ Hence, scaffolds must be biocompatible and must exhibit a porous microstructure to provide support for cell performance.⁶

Ideally, biopolymeric scaffolds should be constructed in a manner that mimics the complex architecture of native tissues. Here, 3D scaffolds must exhibit highly porous structures for cell growth and tissue regeneration. The freeze-drying technique allows to achieve a complex scaffold geometry, as well as high porosity, homogeneous pores, and interconnected ones.⁷ Besides, the porous structure of scaffolds produced by freeze drying affects the ingrowth and replacement of tissue as well as simulating the microstructure of cancellous bone. Kuo *et al.*⁸ fabricated Sr-doped bioactive glass (BG)/chitosan composite scaffolds *via* freeze-drying technique. A porous structure was obtained that met the optimal pore size required for bone TE, allowing the scaffolds to develop bioactivity and cell activity. Further, Nokoorani *et al.*⁹ synthesized graphene-oxide containing poly hydroxyethyl methacrylate (PHEMA)-gelatin scaffolds by freeze-drying, which allowed the constructs to have randomly-oriented interconnected pores.

^aFaculty of Engineering, National University of Mar del Plata, Mar del Plata, Argentina

^bInstitute of Biomaterials, Department of Materials Science and Engineering, University of Erlangen-Nuremberg, Cauerstrasse 6, 91058 Erlangen, Germany. E-mail: farnaz.ghorbani@fau.de; aldo.boccaccini@fau.de; Tel: +49 9131 85-69637; +49 9131 85-28601

^cResearch Institute for Materials Science and Technology, INTEMA (UNMdP-CONICET), Mar del Plata, Argentina



Several cellular processes are influenced by scaffold properties related to the porous architecture (pore size, porosity, and interconnectivity). These characteristics determine the degree to which cells infiltrate a scaffold and control the diffusion of nutrients, metabolites, and waste products.¹⁰ To promote tissue regeneration, the interconnectivity of pores is a critical factor that impacts cell migration and tissue ingrowth.¹¹

One of the challenges of TE is the selection of appropriate materials with chemical composition and mechanical properties similar to those of the target tissue.¹² Natural polymers are capable to provide an excellent performance in biological environments since they possess inherent properties of biological recognition.¹³ Gelatin is a polymer that is formed by hydrolyzing collagen, and is regularly used in bone regeneration due to its hydrophilicity, biodegradability, RGD sequences, simulation of bone's organic matrix phase, and non-immunogenicity.¹⁴ Nouri-Felektori *et al.*¹⁵ showed that the peptide sequence of glycine, proline, and hydroxyproline in gelatin scaffolds boosted bone marrow stem cell attachment and accelerated bone regeneration.¹⁶ However, dissolution rate after interaction with water molecules is promoted, arising from amines and hydroxyl functional groups present in the chemical structure. This problem could be overcome by applying cross-linking techniques.^{16,17} In this context, due to the importance of biomineralization and osteogenic performance in bone regeneration, a bioactive gelatin modifier ((3-glycidyloxypropyl) trimethoxy silane (GPTMS)) is a promising candidate. GPTMS is suitable for chemical cross-linking because it contains amine-friendly coupling agents and hydrolysable functional groups.¹⁸ A water-resistant bond is formed between the oxirane rings of GPTMS and the amino groups of gelatins, thereby cross-linking the structure and forming an organic–inorganic interface.¹⁹ The presence of these bonds creates a nanoscale interaction between the organic and inorganic networks that enhances the *in vivo* stability of scaffolds.²⁰ It has been found that this non-toxic cross-linker can induce biomineralization (hydroxyapatite formation) which is important in bone regeneration.¹⁹

Electroconductive scaffolds started to be a main subject of investigation in recent years due to their great relevance in bio-electronic processes.²¹ Scaffolds containing electrically conductive components, from electroconductive polymeric nanofibers^{22,23} to metal nanoparticles,^{24,25} have been shown to provide a favorable environment for the proliferation of osteoblasts, thereby contributing to accelerating tissue regeneration. This phenomenon can be explained by understanding the bioelectrical properties of bone tissue. Therefore, new strategies for the treatment of injuries and bone tissue diseases can be developed in order to facilitate bone defect repair.²⁶ It has been demonstrated that bone possesses intrinsic piezoelectric properties.²⁷ By compressing the tubular structure of bone during mechanical deformation, a flow of bone-containing ions occurs through the canalicular system, creating a localized electromagnetic field (EMF) that results more intense at thinner sites of the bone due to a greater strain. When the strain-induced EMF is detected, osteoblasts will initiate bone formation.^{27,28} Moreover, electrical stimulation has been shown to influence osteoblast adhesion, proliferation, differentiation, protein synthesis, and finally bone formation by altering the

structure of the cytoskeleton in bone tissue and controlling ion channels.²⁹ It is thus hypothesized that poly(3,4-ethylenedioxythiophene) polystyrene sulfonate (PEDOT:PSS) affects different types of cells and their growth process under electrical stimulation. Based on previous literature, PEDOT:PSS-based scaffolds have also been shown to affect osteogenic differentiation.^{30,31} Guex *et al.*³² demonstrated that freeze-dried scaffolds of pure PEDOT:PSS significantly enhanced gene expression and alkaline phosphatase (ALP) activity in MC3T3-E1 cells after 4 weeks, suggesting that this scaffold could potentially be used in the regeneration of bone tissue.

Surface functionalization strategies can provide a suitable surface for pre-adsorption of proteins and for enhancing cell adhesion, proliferation, and osteogenic differentiation.³³ Accordingly, the dip-coating method can be a suitable strategy due to its simplicity and adaptability to different coating materials as well as the ability to penetrate the pores using suitable coating solutions.³⁴ Considering that the ideal bone scaffold should possess both osteoconductive and osteoinductive properties,³⁵ polydopamine (PDA), a multifunctional mussel-inspired material, has attracted significant attention owing to its potential to support hydroxyapatite (HA) nucleation and growth.³⁶ In addition, PDA serves as a site for anchoring cells and incorporating biological molecules.³⁷ It is possible for dopamine hydrochloride (Dopa-HCl) to spontaneously polymerize in alkaline media.³⁸ In this way, PDA provides active sites for calcium and phosphate ion absorption, thus facilitating the biomineralization of HA.^{36,39} For example, after PDA coating, Chen *et al.*⁴⁰ demonstrated that not only was the formation of HA on poly(L-lactide) fibrous membrane significantly accelerated, but also their hydrophilicity was greatly improved. PDA was also found to contribute to an improved adhesion and proliferation of MC3T3-E1 cells as well as to the upregulation of ALP activity and the expression of osteogenic-related genes.

Herein, silane-modified gelatin-PEDOT:PSS scaffolds were fabricated by the freeze-drying technique and functionalized through polymerization of Dopa-HCl in alkali conditions. This study was conducted in order to fabricate electroconductive scaffolds that can be coated with PDA to promote physicochemical, mechanical, and *in vitro* properties for bone regeneration. A synergistic effect between PDA and GPTMS is also expected to induce bioactivity and osteogenic performance. To characterize the scaffolds, microstructural and chemical analysis, electrical conductivity, mechanical strength, water–scaffold interactions, biodegradation behavior, and biomineralization potential were studied. Furthermore, hybrid constructs have been studied *in vitro* for understanding the influence of PDA functionalization on cell adhesion, proliferation, ALP expression, and HA production in order to create an appropriate structure for further experiments on bone regeneration *in vitro* and *in vivo*.

2. Materials and methods

2.1. Materials

Gelatin from porcine skin (Type A, gel strength 300), dopamine hydrochloride (Dopa-HCl, $M_w = 189.64 \text{ g mol}^{-1}$), 3-



glycidyloxypropyl trimethoxysilane (GPTMS, $M_w = 236.34$ g mol $^{-1}$), poly(3,4-ethylenedioxythiophene) poly(-styrenesulfonate) (PEDOT:PSS, 3–4%, $d = 1.011$ g cm $^{-3}$), hydrochloric acid (HCl, $M_w = 36.46$ g mol $^{-1}$), potassium phosphate dibasic ($M_w = 174.2$ g mol $^{-1}$), penicillin-streptomycin (suitable for cell culture, lyophilised), and Bradford reagent (for 0.1–1.4 mg ml $^{-1}$ protein) were purchased from Sigma-Aldrich (Germany). Tris ($M_w = 121.14$ g mol $^{-1}$) was purchased from ROTH Co (Germany). SBF solution was prepared with calcium chloride and potassium phosphate dibasic trihydrate, purchasing from Sigma-Aldrich (China and Germany, respectively); sodium hydrogen carbonate and potassium chloride from EMSURE® (Germany); magnesium chloride hexahydrate from Honeywell Fluka Co. (Germany) and Sodium sulphate anhydrous from VWR Chemicals (Belgium). DPBS (Dulbecco's Phosphate Buffered Saline, 1×), trypan blue stain (0.4%) and Hank's Balanced Salt Solution (HBSS) were purchased from Gibco Co. (Germany). Calcein-AM was purchased from Invitrogen, USA. OsteoImage™ mineralization assay was purchased from Lonza, USA. MG-63 cells (biological source: human bone; description: human osteosarcoma) (Sigma-Aldrich, Germany) were obtained from the available cell bank (Institute of Biomaterials, University of Erlangen Nuremberg).

2.2. Preparation of gelatin-PEDOT:PSS scaffolds

Gelatin-PEDOT:PSS scaffolds were prepared by the freeze-drying technique. The polymeric solution was prepared by adding 1% (w/v) PEDOT:PSS to a 3% (w/v) gelatin solution. After complete dissolution, the silane coupling agent (gelatin : GPTMS weight ratio 1 : 0.5) was added the polymeric solution. After 2 h aging, the solution was poured into molds. Frozen samples at -20 °C were then lyophilized for 3 days.

2.3. PDA decorated gelatin-PEDOT:PSS scaffolds

Gelatin-PEDOT:PSS scaffolds were coated with PDA by a dip-coating method. In order to accomplish this, scaffolds were soaked for 24 hours in media containing 2 mg ml $^{-1}$ Dopa-HCl solution dissolved in 10 mM Tris buffer (pH 8.5) in isopropanol–water medium (5 : 2 volume ratio) in a dark environment. Then, washed samples were lyophilized for 3 days.

2.4. Characterizations

2.4.1. Morphology observations. The morphology of the scaffolds was observed with a field-emission scanning electron microscope (FE-SEM, 1550VP Gemini, Carl Zeiss™, Germany) at an energy of 1 kV. Before FE-SEM observation, a thin layer of gold was coated on the samples to prevent the charging effects and obtain a conductive surface. FE-SEM images were also used to quantify the pore size using KLONG Image Measurement (KLONG Image Measurement Light, Edition 11.2.0.0).

2.4.2. Fourier transform infrared spectroscopy. Fourier Transform Infrared spectroscopy (FTIR, IRAffinity, 1S-Shimadzu, Japan) was done in transmission mode at the wavenumber ranging from 4000 cm $^{-1}$ to 400 cm $^{-1}$ wavenumber at a resolution of 4 cm $^{-1}$.

2.4.3. Conductivity. The resistivity (R) of the polymeric scaffolds was measured by a Low Resistivity Meter (Loresta AX MCP T370, Nittoseiko Analytech, Japan) device. The equipment measures the volume resistivity of the sample (ρ_v) and the resistivity has been determined using eqn (1).⁴¹

$$R[\Omega] = \frac{\rho_v[\Omega\text{cm}]}{RC_F v t[\text{cm}]} \quad (1)$$

where, t is the thickness of the sample and $RC_F = 3.014$ is the error factor of the device. In order to obtain a successful resistance measurement, scaffolds were immersed in PBS solution for five seconds.

2.4.4. Mechanical strength. To study the mechanical properties of the dry gelatin-PEDOT:PSS and PDA-coated ones, cylindrical scaffolds were tested in dry condition by a strength testing system (INSTRON 5967, USA) equipped with a 100 N load cell under a crosshead speed of 0.5 mm min $^{-1}$.

2.4.5. Water-scaffold interactions. A drop shape analyzer (DSA30 Expert, Kruss, Germany) was used to perform the sessile drop method at room temperature in order to evaluate the interaction of water molecules with scaffolds and the influence of PDA coatings on hydrophilicity of samples (Kruss DSA 100, Germany).

Water uptake tests were conducted to evaluate scaffolds' capacity to absorb water. Therefore, scaffolds were weighed and later immersed in 15 ml PBS solution at 37 ± 0.5 °C for 2, 4, 6 and 24 h. At each time interval, samples were weighed again after removing them from the PBS solution. The absorption capacity was calculated according to eqn (2),⁹ where W_0 is the initial weight and W is the wet weight of the specimen:

$$\text{Water uptake}(\%) = \left[\frac{(W - W_0)}{W_0} \right] \times 100 \quad (2)$$

2.4.6. Hydrolytic biodegradation. The biodegradation rate of the composite scaffolds was determined after immersing the samples in 15 ml of PBS solution at 37 ± 0.5 °C for 4 weeks at a rotational speed of 60 rpm. Initially, scaffolds were weighed, and at the end of each week, samples were washed with distilled water, and then lyophilized to obtain their dry weights. The buffer was refreshed weekly. The weight loss rate was calculated using eqn (3),⁴² where W_0 and W are the initial and final dry weight of the scaffolds:

$$\text{Weight loss}(\%) = \left| \left[\frac{(W - W_0)}{W_0} \right] \right| \times 100 \quad (3)$$

2.4.7. Biominerization. A biominerization assay was carried out in order to examine the potential of scaffolds in the formation of HA-like layers on surfaces. Scaffolds were immersed in 15 ml SBF solution at 37 ± 0.5 °C under a rotational speed of 60 rpm for 4 weeks.⁴³ The SBF solution was refreshed every 2 days. After 4 weeks, scaffolds were washed with distilled water and lyophilized. The structure of the mineralized layer on the surface and crystalline phases was evaluated by FE-SEM, X-ray diffraction (XRD, Rigaku-Mini flex, Germany), and FTIR.

2.4.8. Cell-scaffold interactions. The performance of the cells in contact with scaffolds was evaluated following MG-63 cell culture on the samples. First, the scaffolds were sterilized with UV light for 1 h and then were seeded using 10 000 MG-63 cells/ml in DMEM supplemented with 10% FBS, 1% U per ml penicillin-streptomycin. They were then incubated for 2 days at 37 ± 0.5 °C, 5% CO₂, complemented by a 95% humidity. The cultured cells were fixed with glutaraldehyde and formaldehyde solutions after two days of culture. Afterwards, the specimens were dehydrated with ethanol series and allowed to dry in the open air prior to being observed by FE-SEM.

The viability of MG-63 cells was evaluated using Calcein-AM staining assays after 2, 4, and 7 days of culture. The cell-seeded scaffolds were incubated in a solution of 4 µl calcein-AM per ml HBSS for 1 h at 37 ± 0.5 °C, 5% CO₂, and 95% relative humidity. At each time interval, the viability of the cells was monitored with a fluorescence microscope (Axio Observer, Carl-Zeiss, Germany).

The proliferation of MG-63 cells on freeze-dried gelatin-PEDOT:PSS scaffolds before and after PDA coating was assessed using the WST-8 assay after 2, 4 and 7 days of culture. After culturing the cells, the medium was removed, and the samples were washed with HBSS solution. Afterward, cell loaded scaffolds were incubated for 3 h in 3% WST-8 solution (at 37 °C, 5% CO₂, and 95% humidity). Hereafter, the absorbance of the medium was measured by a plate reader machine at 450 nm (FLUOstar Omega, BMG Labtech, Germany).

ALP activity was measured after 7 and 21 days of cell culture. Following lysis of the cells with lysis buffer, the medium was centrifuged at 1200 rpm at each time interval. Upon addition of the supernatant to an ALP-mix solution containing p-NPP, the solution was incubated for 180 minutes. The reaction was stopped by adding NaOH. ALP activity was measured by analyzing absorbance at wavelengths of 405 and 690 nm. The absorbance related to these peaks is proportional to the ALP activity. As a final adjustment, the Bradford assay was used to determine the total protein content.

An OsteoImage™ Mineralization Assay by Lonza kit was used to assess the HA content of bone-like nodules formed by cells. Following the instructions in the kit, the cells were washed twice with wash buffer solution after 21 days. Mineralization in the cells was monitored using a fluorescence microscope and a fluorescent microplate reader following staining in dark conditions.

2.5. Statistical analysis

Each experiment was repeated five times and data were reported as the mean \pm standard deviation. The significance of the average values was calculated using a *t*-test calculator; *p* \leq 0.05 was considered significant.

3. Results and discussion

3.1. Morphology observations

One of the most important parameters influencing osteogenesis is the scaffold porous structure. The scaffold's structure

facilitates nutrients' diffusion and exchange as well as the infiltration of the ECM into the bone tissue when it is sufficiently interconnected.

Fig. 1A illustrates schematically the silane cross-linked gelatin-PEDOT:PSS scaffold preparation and surface modification *via* PDA. According to FE-SEM micrographs (Fig. 1B and C), both unmodified and modified constructs displayed hierarchically and interconnected pores ranging from micron to nanometers. As a result of the surface modification, a homogeneous layer of PDA was deposited on the surface (Fig. 1C), resulting in a rougher surface. It is similar to the findings obtained by Zhuang *et al.*⁴⁴ and Xu *et al.*⁴⁵ in which a PDA layer coating on the surface of the scaffold indicated starting self-oxidative spontaneous polymerization of Dopa-HCl. As shown by Han *et al.*⁴⁶ successful PDA deposition on the scaffold can be determined by the change in color from light blue to dark brown.

As a result of the PDA coating, the average pore size decreased substantially from 239 ± 39 µm to 122 ± 39 µm (Fig. 1E). As deposited PDA adheres to the inner wall of scaffolds, it narrows pore sizes, thus making the difference between coated and uncoated scaffolds statistically significant. Similar observations were made by Kasemset *et al.*⁴⁷ It is evident from the considerable standard deviation of the mentioned measurements that there are differences in pore sizes between freeze-dried scaffolds with and without coatings. Several studies have shown that pores of 100–200 micrometers facilitate the formation of mineralized bone by osteoblast activity following implantation.^{46,48} Such pores allow macrophages to infiltrate, eliminate bacteria, and promote vascularization *in vivo*. Meanwhile, smaller pores (<100 µm) are associated with the formation of non-mineralised osteoid or fibrous tissue.⁴⁹

3.2. Fourier transform infrared spectroscopy

In order to evaluate chemical composition and functional groups of raw materials and composite scaffolds, as well as to confirm PDA layer deposition, FTIR analysis was carried out, as shown in Fig. 2A. The gelatin characteristic peaks were identified and located at 1640 cm⁻¹, 1535 cm⁻¹, and 1240 cm⁻¹, respectively, corresponded with amide I (C=O stretching), amide II (N-H bending and C-N stretching), and amide III (C-N stretching).⁵⁰ The peak at 3282 cm⁻¹ represents the stretching vibration of the N-H (Amide A) and O-H (Amide B).⁵¹ As a result of comparing the pure gelatin peaks with the composite scaffolds, the characteristic peaks of an effective cross-linking between gelatin and GPTMS can be determined by detecting Si-O-Si (1030 cm⁻¹ and 1080 cm⁻¹ respectively) and Si-OH (905 cm⁻¹).^{52,53} Here, a reaction occurs between the oxirane rings on GPTMS and the amine functional groups of gelatin. Hydrolyzing the trimethoxy groups in the GPTMS chemical structure leads to formation of pendant silanol groups (Si-OH) under acid-catalyzed reaction.⁵⁴ Si-O-Si bonds form during the evaporation of the solvent when Si-OH bonds are converted to Si-O-Si bonds, resulting in interchain covalent bonds and cross-linked structure.⁵⁵



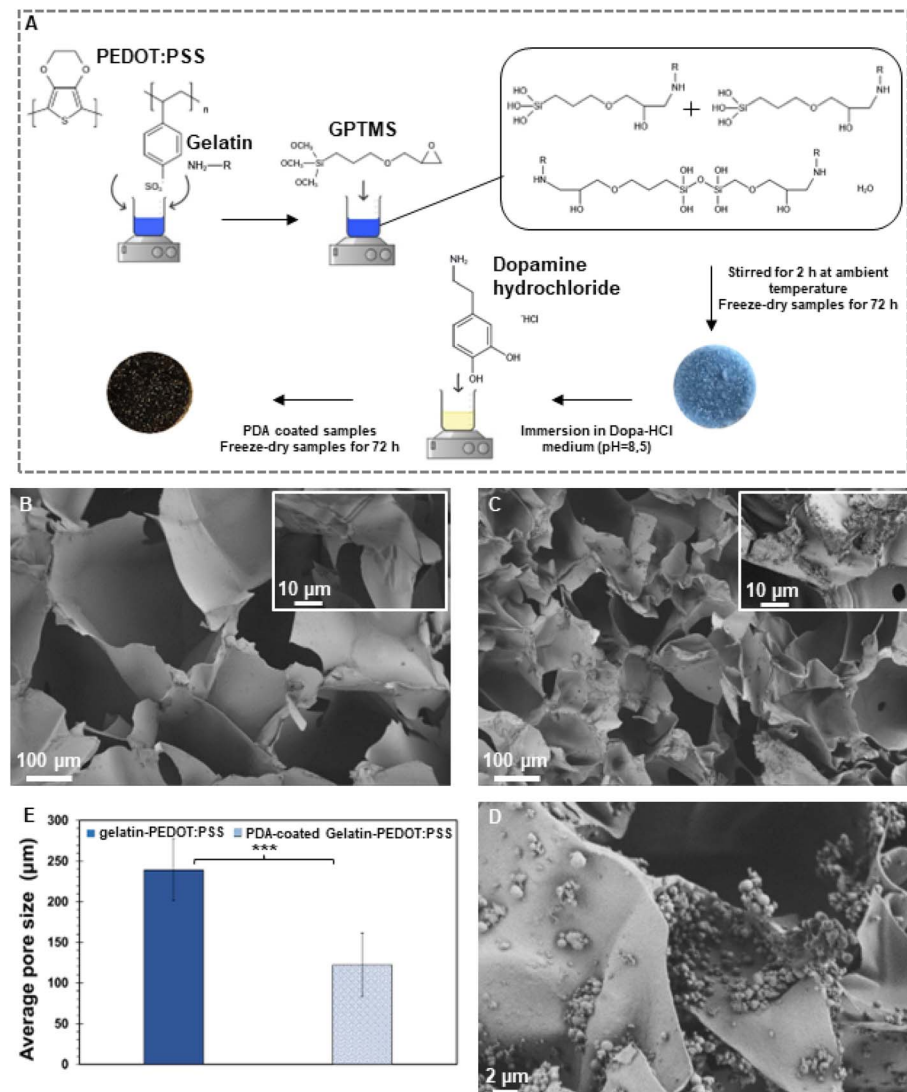


Fig. 1 Morphological evaluation of the synthesized scaffolds. (A) Schematic of fabrication process. (B) FE-SEM micrographs of gelatin-PEDOT:PSS and (C and D) PDA-coated gelatin-PEDOT:PSS constructs. (E) Average pore size of modified and un-modified scaffolds. (Difference is extremely statistically significant ($***p < 0.001$)).

It was found that the characteristic absorption peaks of PEDOT:PSS were located at 1161 cm^{-1} (sulfonic acid group of PSS), $1030\text{--}1085\text{ cm}^{-1}$ (C—O—C stretching), $930\text{--}1000\text{ cm}^{-1}$ (C—S stretching), and 1272 cm^{-1} (C=C and C—C stretching of the quinoidal structure of PEDOT).⁵⁶ Moreover, a broad peak between $3200\text{--}3400\text{ cm}^{-1}$ indicates the O—H stretching and a peak at 1630 cm^{-1} shows C=C bonds from both PEDOT and phenyl group of PSS.⁵⁷ FTIR spectra of both types of scaffolds show thus characteristic peaks of PEDOT:PSS: the broad peak between $3200\text{--}3400\text{ cm}^{-1}$ and one more intense peak at 1165 cm^{-1} corresponding to the sulfonic acid group of the PSS.

The PDA peak at 1120 cm^{-1} corresponds to the stretching vibration of C—O.⁵⁸ It is found that the vibrations of OH are detected at 1345 cm^{-1} and 1285 cm^{-1} , respectively. Characteristic peaks at 1600 cm^{-1} and 1510 cm^{-1} are indicative of N—H vibrations of amines.⁵⁹ Hydroxyl and N—H bonds in the catechol groups are recognized by a broad peak between 3200 and

3500 cm^{-1} .⁶⁰ PDA polymerization involves several complex steps including oxidation, cyclization, and re-arrangement of the Dopa-HCl molecule. An oxidation reaction results in the formation of dopaminequinone, which is then cyclized *via* a Michael addition reaction.⁵⁹ A further oxidation of this species leads to the formation of 5,6-dihydroxyindole. PDA is formed by the interaction of unreacted catechol groups with *o*-quinone of 5,6-dihydroxyindole, and as a consequence, the obtained molecule has both catechol and quinone groups, which are considered to be the main structural components of PDA.³⁹

A covalent bond between PDA and gelatin molecules is formed when PDA is coated on gelatin-PEDOT:PSS scaffolds. A Michael type addition reaction can also be described as this reaction. Specifically, new O—H and N—H bonds are formed between the quinone of PDA and the amine group of gelatin, identified by a broad peak between 3200 and 3400 cm^{-1} . In addition, PDA-coated gelatin-PEDOT:PSS samples exhibited

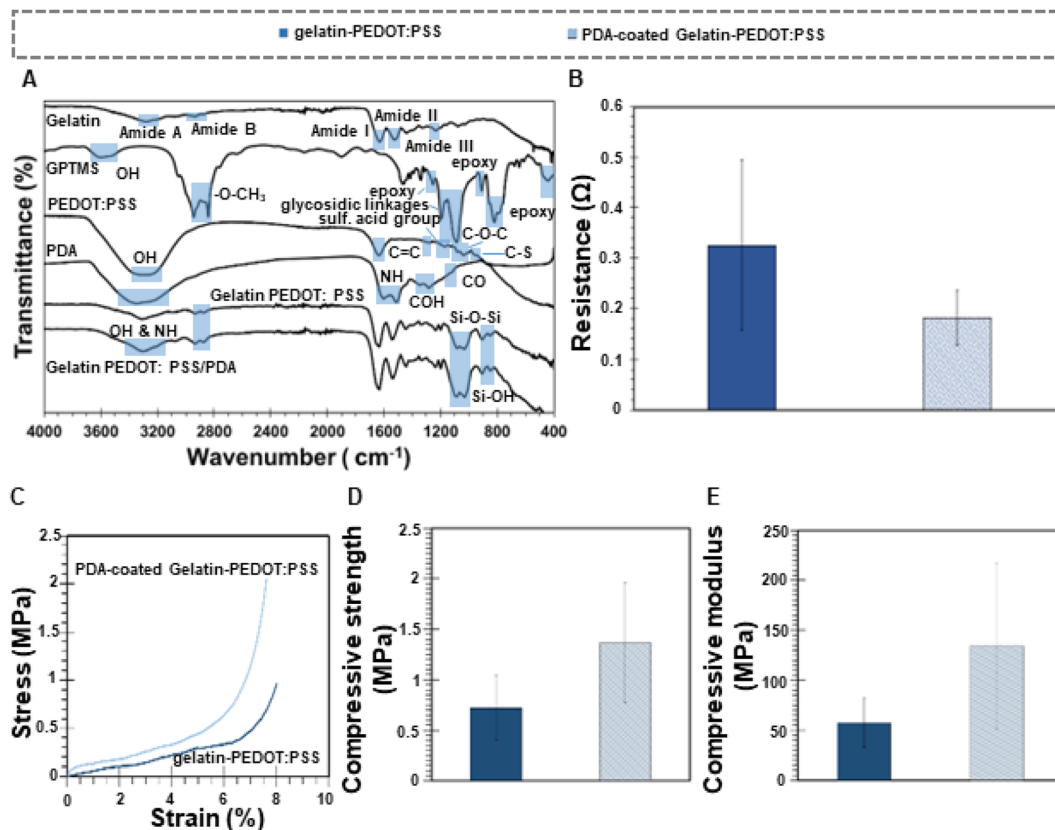


Fig. 2 Chemical, electrical and mechanical characterization of scaffolds. (A) FTIR spectra of raw materials and scaffolds showing the main peaks. (B) Electrical conductivity of the constructs. (C) Stress–strain curve, (D) Compressive strength and (E) compressive modulus for coated and uncoated scaffolds.

mainly gelatin peaks, although NH and OH bonds, indicating a new polymer deposition, were visible in the PDA peaks.

3.3. Electrical conductivity

A direct relationship exists between the electrical potential and the ion flux across cell membrane.⁶¹ Polarizing a cell generates an electric field that alters the voltage across the membrane, changing the electrical conductivity of adjacent cells and causing other cells to coordinate their actions. Thus, the conductivity of the scaffold can facilitate communication between cells in response to electrical stimulation. There is evidence that either periodic electrical stimulation at different voltages or different types of current can induce osteogenic differentiation in human fetal and mesenchymal stem progenitor cells.⁶² In this regard, Gittens *et al.*⁶³ evaluated MG-63 cells differentiation at polarized surfaces and realized that varying the voltage of the electric stimulation resulted in an optimal rate of osteoblast differentiation.

As a means of achieving higher stimulation and more efficient regeneration of bone, conductive materials such as PEDOT:PSS can be incorporated in the constructs, which can ideally promote *in vitro* osteogenesis and *in vivo* bone regeneration following biomaterial implantation.³² As observed in Table 1 and Fig. 2B, conductivity of scaffolds was $(320 \pm 240) \times 10^{-3}$ S cm⁻¹ and $(490 \pm 250) \times 10^{-3}$ S cm⁻¹ for uncoated and

PDA coated scaffolds, respectively. Conductivity values for cancellous and cortical bone are around $1.6\text{--}2.0 \times 10^{-3}$ S cm⁻¹ and $5.8\text{--}6.3 \times 10^{-4}$ S cm⁻¹, respectively.²⁹ Therefore, conductivity of non-coated scaffolds are at least 40 times greater than the most conductive part of bone. Nevertheless, several studies have shown that high electroconductive constructs also make a positive impact in regeneration of bone since they can boost electrical signaling among the cells. For instance, Shahini *et al.*⁶⁴ indicated that cell metabolism can be enhanced by high conductive scaffolds. Electroconductive scaffolds increase the cytoplasmic content of cells, indicating that they are suitable for cell attachment and proliferation. A reproducible increase in extracellular matrix traces in the conductive scaffolds suggests that human mesenchymal stem cells were highly active on electroconductive scaffolds, possibly due to improved intracellular electrical signaling between them. Gopinathan *et al.*⁶⁵ synthesized poly- ϵ -caprolactone (PCL) scaffolds with different concentrations of carbon nanofillers (CNF) and demonstrated that samples with 10% w/w CNF showed the highest electrical conductivity (up to 19 S m⁻¹), helping the communication, attachment, and proliferation of human meniscal cells. On the other side, Shadjoul *et al.*⁶⁶ showed that bioactive glass and graphene nanoplatelet composites with high electroconductivity (13 S m⁻¹) did not negatively affect the bioactivity performance of the constructs, enabling bone tissue engineering.

Table 1 Conductivity values of both PDA-coated and uncoated scaffolds in comparison with natural bone

	Cortical bone	Cancellous bone	Gelatin-PEDOT:PSS	PDA-coated gelatin-PEDOT:PSS
Conductivity [S cm ⁻¹]	(5.8–6.3) × 10 ⁻⁴	(1.6–2.0) × 10 ⁻³	(320 ± 240) × 10 ⁻³	(490 ± 250) × 10 ⁻³

As a result of surface modification, PDA-coated scaffolds showed a greater conductivity than uncoated scaffolds. A similar result was found by Xie *et al.*⁶⁷ in which PDA was incorporated into pure polypyrrole microcapsules to improve their conductivity. This might be due to the semiconductor nature of the PDA-coated scaffolds, since the semiconductor is composed of aromatics and conjugated molecules, both the conductive and valence bands are characterized by the π -system.⁶⁸ In consequence, the charge transfer would result in a higher conductivity.

3.4. Mechanical properties

Bone TE scaffolds should temporarily fulfill the structural functions of native bone: they should be strong and stiff enough to withstand the loads that will occur *in vivo* at the implantation site. Otherwise, in the case of scaffolds with lower mechanical properties, the regeneration process is compromised if the scaffolds collapse during implantation. It is well known that the type of material and microstructure, such as pore structure and morphology, have a significant impact on mechanical properties³⁷

Fig. 2C–E depicts the stress–strain curve and mechanical properties (compressive stress and elastic modulus) of PDA coated and uncoated gelatin-PEDOT:PSS scaffolds. Considering the area under the stress–strain curve, PDA coating improved the toughness of the samples. For un-coated scaffolds the toughness was 80.68 GJ m⁻³, whereas for PDA-coated constructs it was 137.95 GJ m⁻³. Additionally, the compressive stress and Young's modulus of gelatin-PEDOT:PSS scaffolds were (0.7 ± 0.3) MPa and (57 ± 24) MPa, respectively. Upon applying PDA coating, the compressive stress increased by 40% (1.4 ± 0.6 MPa), while the elastic modulus increased by around 145% (134 ± 83 MPa). Similarly, Shen *et al.*⁶⁹ have demonstrated improved mechanical properties and a reduction in average pore size after PDA coating of alginate scaffolds. Human cancellous bone exhibits compressive strength values ranging from 0.1 MPa to 16 MPa, and elastic modulus values in the range 50 MPa to 500 MPa.⁷⁰ Thus the present scaffolds exhibit adequate mechanical stability for cancellous bone TE applications by mimicking the compressive strength and elastic modulus of cancellous bone.

As a result of chemical equilibrium in aqueous solutions, the PDA molecule shifts between catechol and quinone. Under alkaline conditions, the equilibrium shifts to quinone, conferring the PDA molecule a great affinity for the amine groups of proteins.⁷¹ Gelatin forms covalent bonds with PDA when its primary amines come into contact with the quinones. Consequently, catechol groups will form, establishing a strong bond with gelatin.⁷² Accordingly, PDA plays a key role in the enhancement of physical properties and cross-linking points,

resulting in better mechanical properties of the scaffold due to stronger binding between the networks within the hydrogel.

3.5. Water–scaffold interactions

Wettability of bone scaffolds plays a significant role in their biological behavior. This property not only promotes adsorption of blood and serum proteins, but it is also essential to improving osseointegration.

The hydrophilic properties of PDA coated and uncoated gelatin-PEDOT:PSS scaffolds were evaluated using water contact angle measurements (Fig. 3A). The average value of contact angle for gelatin-PEDOT:PSS scaffolds was found to be 101° (Fig. 3Ai). PDA coated samples displayed a 45° water drop contact angle that absorbed after 10 seconds (Fig. 3Aii and iii, respectively). It appears that the gelatin-PEDOT:PSS scaffolds coated with PDA had a highly hydrophilic surface. Similarly, Ku *et al.*⁷³ found rapid water absorption due to the high hydrophilicity of PDA. Shen *et al.*⁷⁴ demonstrated that such surfaces can adsorb proteins like laminin, providing a better substrate for cell adhesion.

On the other hand, PBS absorption capacity was evaluated as a function of time in order to analyze the interaction between water and the scaffold in freeze-dried gelatin-PEDOT:PSS and PDA-coated scaffolds. Fig. 3 illustrates that after 2 h, both gelatin PEDOT:PSS and PDA-coated scaffolds absorbed a large amount of PBS solution. The values obtained were (730 ± 327)% and (1462 ± 212)% respectively for gelatin PEDOT:PSS and PDA-coated scaffolds, and the difference in absorption was statistically significant. After 24 hours, both scaffolds showed gradual increases in PBS absorption, until an equilibrium was reached. It was found that the absorbance values of gelatin-PEDOT:PSS scaffolds coated with PDA were approximately 41% higher than those of uncoated scaffolds. Amine and catechol functional groups in the PDA enhance the water uptake capacity of constructs. According to Patra *et al.*,⁷⁵ PDA coating improves water absorption capacity and therefore, provides a hydrophilic construct for better cellular interactions, resulting in a high level of extracellular matrix (ECM) formation.

3.6. Biodegradation

Structural stability and degradation behavior of scaffolds as well as the biocompatibility of the by-products are important issues dictating the success of scaffolding. Although the mechanical properties of scaffolds should be sufficiently high during the regeneration process, they also need to degrade at an appropriate rate during tissue formation according to the growth rate of the new tissue. The mechanism and kinetic of biodegradation are affected by a variety of factors including chemical composition, hydrophilicity, pore size and shape, and surface area.¹⁷



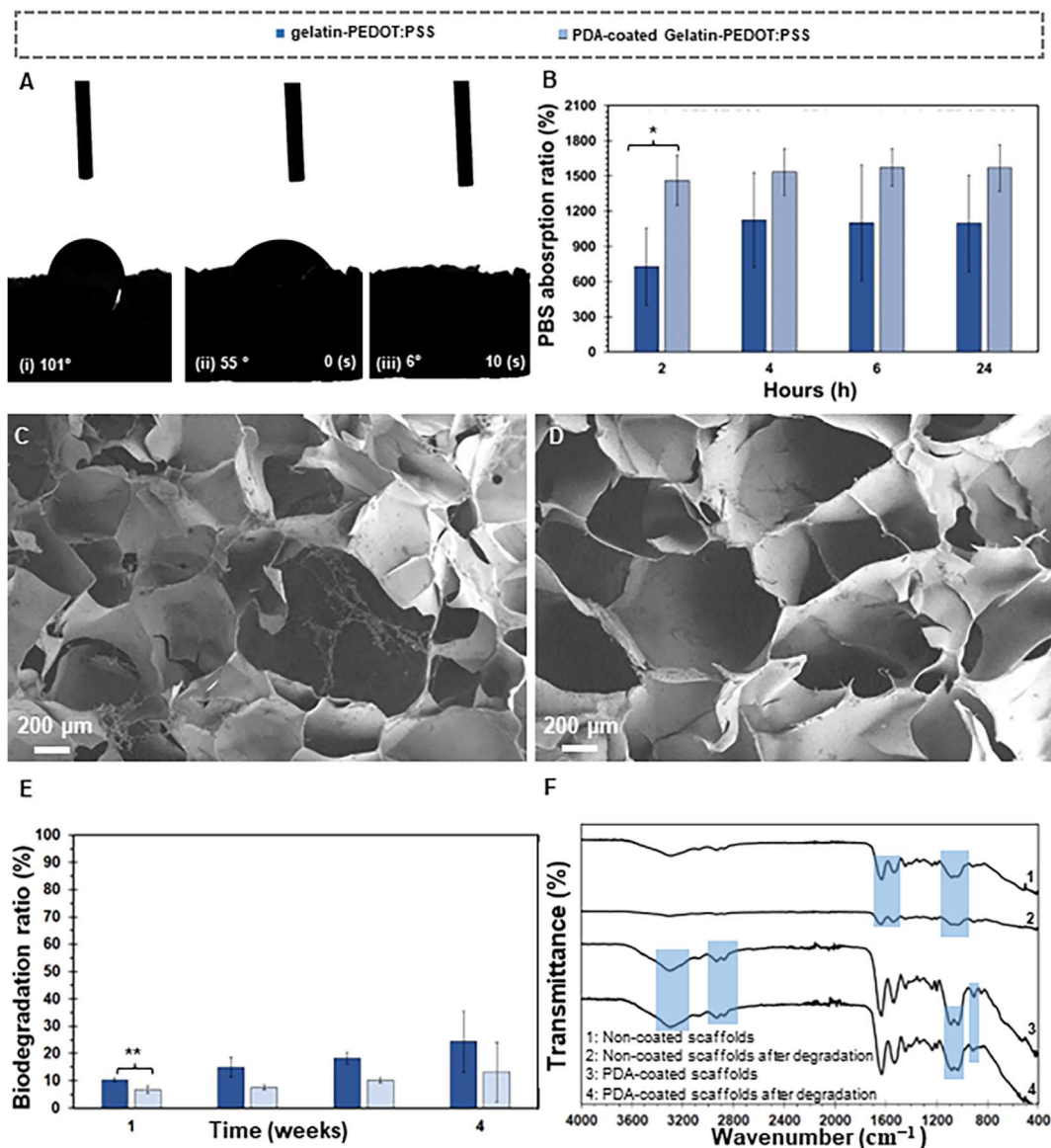


Fig. 3 Scaffolds-water interactions. Water-drop contact angle test of (Ai) gelatin-PEDOT:PSS and (Aii and Aiii) sequence of drop absorption for PDA-coated gelatin-PEDOT:PSS. (B) PBS absorption capacity and (C–F) biodegradation behavior of scaffolds. (C and D) FE-SEM micrographs of (C) un-coated and (D) PDA coated gelatin-PEDOT:PSS scaffolds, (E) Biodegradation ratio and (F) FTIR spectra of both PDA-coated and uncoated scaffolds before and after degradation. (Differences resulted statistically significant ($*p \leq 0.05$) and very statistically significant ($**p < 0.01$)).

Fig. 3C–E show FE-SEM micrographs of degraded gelatin-PEDOT:PSS and PDA coated constructs, along with degradation rates for different immersion times in PBS solution. As a result of immersion of scaffolds in PBS solution for four weeks, the gelatin-PEDOT:PSS scaffolds showed signs of degradation, such as loosened pore walls, and there was a higher degree of damage to the microstructure than in the PDA-coated scaffolds. PDA surface modification showed a remarkable influence on the degradation resistance of scaffolds, which means that scaffolds coated with PDA degraded at a slower rate than uncoated scaffolds. There was a statistically significant difference between the rates of degradation of PDA-coated samples ($7 \pm 1\%$) and uncoated samples ($10 \pm 1\%$) after one week. For surface-modified scaffolds, the biodegradation

rate after 2 weeks reached ($8 \pm 1\%$), after 3 weeks it was ($10 \pm 1\%$). It shows biodegradation rates of the pure scaffolds were faster than those of the PDA-coated scaffolds. Un-coated scaffolds degrade 19.6% more rapidly after two weeks than coated scaffolds, followed by a 41.5% increase after three weeks, and a 51.3% increase after four weeks. Surface modified scaffold degradation rates were less than 15% after four weeks, consistent with a steady gradient. Pore size reduction and improved mechanical stability of scaffolds after coating with PDA can be a possible reason for this behavior. Here, a direct relationship appears to exist between the rate of bone degradation and the rate of bone formation. In damaged tissue, cartilaginous calluses form within two weeks. It generally takes two months for the defect site to undergo endochondral ossification after

the cartilaginous calluses have been bridged. Following the initiation of bone regeneration, bone remodeling can begin as early as three to four weeks later.⁷⁶

A reduction in the intensity of the characteristic peaks in gelatin-PEDOT:PSS constructs after 4 weeks is consistent with the degradation of the constructs (Fig. 3F). Specifically, peaks related to GPTMS cross-linking of gelatin in uncoated scaffolds such as Si–O–Si and Si–OH bonds at 1030 cm^{-1} , 1080 cm^{-1} and 905 cm^{-1} showed a reduction in intensity after immersion of scaffolds in the PBS solution. In addition, characteristic amide peaks of gelatin (1640 cm^{-1} for Amide I, 1535 cm^{-1} for Amide II) as well as OH and NH peaks at 3200 to 3500 cm^{-1} showed reduction in uncoated samples after a 4 week degradation

period. PDA-coated scaffolds maintained mainly the intensity of OH and NH characteristic peaks as well as amide I and II. Although the intensity of some characteristic peaks in coated scaffolds was reduced, it was less than the observed reduction in uncoated samples, indicating enhanced stability and long-term durability of the scaffolds after surface modification.

In aqueous media, gelatin is degraded through the process of hydrolysis, and its cross-linking with GPTMS enhances its resistance to degradation, as demonstrated by Nouri-Felekori *et al.*⁷⁷ Furthermore, other studies confirmed that the addition of PEDOT:PSS into gelatin/BG scaffolds increases the chemical stability and, consequently, the biodegradability resistance of the composites.⁶⁴ However it needs to be considered that there

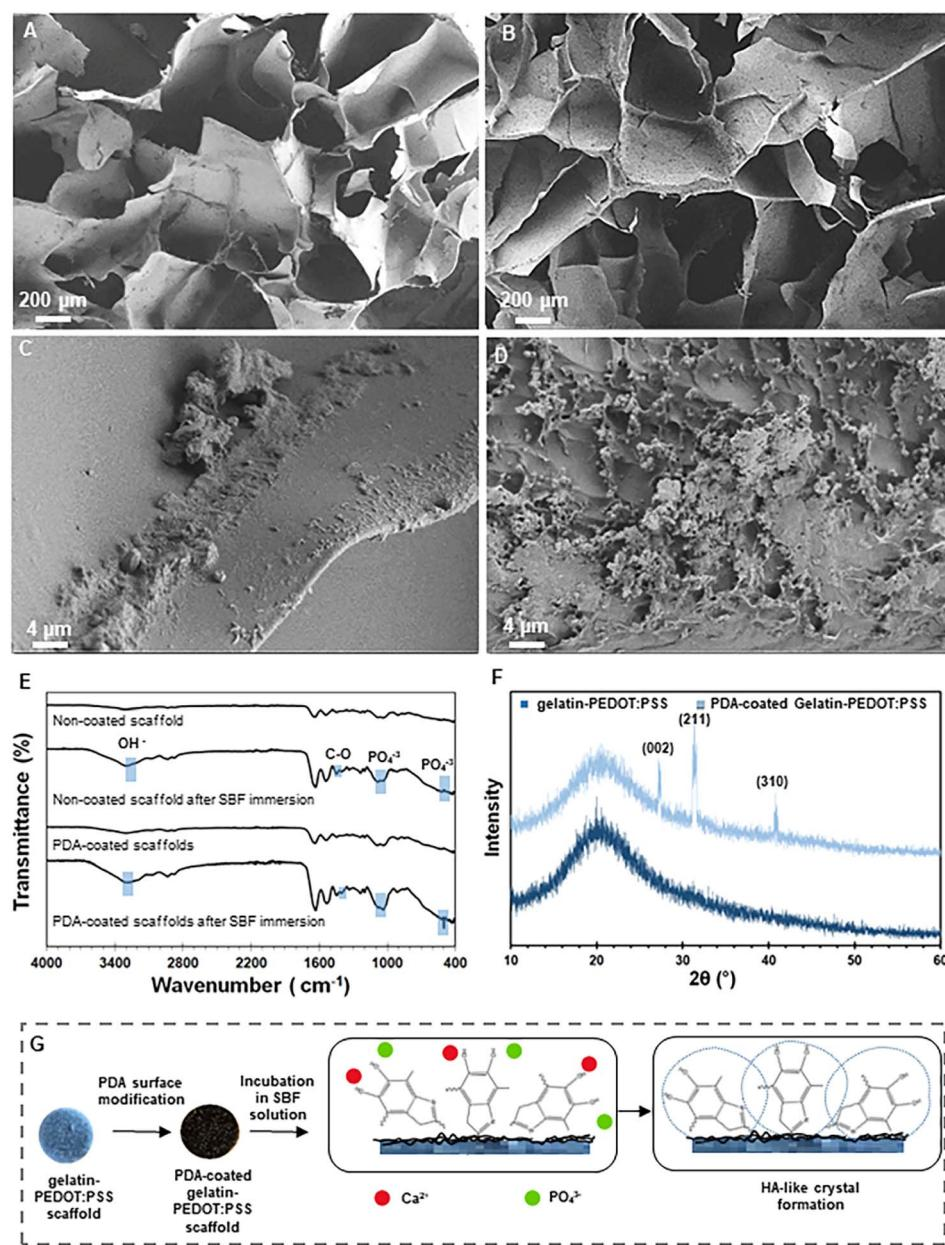


Fig. 4 Bioactivity of the constructs. (A–D) FE-SEM micrographs ((A, C) gelatin-PEDOT:PSS and (B, D) PDA-coated gelatin-PEDOT:PSS scaffolds), (E) FTIR spectra and (F) XRD patterns of mineralized HA-like layer on the surface of PDA modified and unmodified scaffolds after 4 weeks of immersion in SBF solution. (G) Representation of bioactivity mechanism.



are ester linkages in this copolymer that degrade *via* hydrolysis.⁷⁸ As indicated, coating the gelatin-PEDOT:PSS constructs with PDA also improved their mechanical properties and their ability to resist biodegradation. Previously, we have demonstrated a positive effect on controlling the biodegradation rate of alginate dialdehyde-gelatin scaffolds when modified with PDA.⁷⁹ Many molecules in the human body, including H₂O₂, microorganisms, and free radicals, can cause oxidative degradation of PDA molecules.⁶⁸ Besides, Vona *et al.*⁸⁰ demonstrated that PDA coating of living diatom microalgae also enhanced their degradation resistance in acidic media.

3.7. Bioactivity

In the content of materials that will be in contact with bone, bioactivity refers to a material's ability to nucleate and grow HA layers on its surface and it needs to be considered when designing a scaffold for bone regeneration.⁸¹ An *in vitro* experiment using SBF was performed in order to determine the acellular bioactivity behavior of the fabricated constructs. Fig. 4A–D show FE-SEM micrographs after 4 weeks of immersion in SBF. There is a relatively thin layer of HA-like material on the surface of gelatin-PEDOT:PSS scaffolds, as shown in Fig. 4A and C. It has been shown that silane coupling agents, such as GPTMS, can positively influence the bioactivity behavior of constructs due to the presence of Si ions, and therefore this compound can stimulate the growth of apatite.⁸² However, a comparison of the FE-SEM micrographs revealed significant HA deposition on the PDA-modified matrix. Another study has shown that nano-hydroxyapatite particles coated with PDA and incorporated into PCL matrix create a bioactive and cytocompatible scaffold that accelerates the formation of apatite layers.⁸³ At the same time, in Dimassi *et al.* study⁸⁴ the formation of spherical particles on the surface of PDA-coated chitosan nanofibers was observed and analyzed by XRD and FE-SEM.

Fig. 4E shows the FTIR spectra before and after immersion of PDA-coated and uncoated gelatin-PEDOT:PSS scaffolds in the SBF solution in order to analyze the *in vitro* acellular bioactivity. After bioactivity test, the spectra of scaffolds reveal a broad band from 3572 cm^{−1} to 3140 cm^{−1}, which indicates the typical stretching mode of OH groups.⁸⁵ The fact that the twin peak at 1080 cm^{−1} (corresponding to PO₄^{3−}) in the PDA-coated samples has been replaced by a single peak⁸⁶ is an indication of crystallization of the apatite. A greater intensity of the peak is evident for scaffolds modified with PDA. Peaks at 500 and 1050 cm^{−1} are attributed to PO₄^{3−} and C–O asymmetric stretching is observed at 1400 cm^{−1}.⁸⁷ After immersion of samples in SBF, calcium phosphate rich crystalline layers are shown on the surface of both type of scaffolds. Nevertheless, PDA-coated samples displayed a higher intensity of the characteristic HA peaks. Consequently, PDA-modified constructs showed promising results with respect to their bioactivity.

Fig. 4F illustrates the XRD patterns of the gelatin-PEDOT:PSS and PDA-coated scaffolds. All scaffolds displayed a broad peak at 20°, representing the amorphous nature of polymeric materials. The appearance of XRD reflection peaks at 2θ angles of 26.7°, 30.9° and 42° correspond to (002), (211) and (310)

reflections of apatite (JCPDS #09-0432), respectively, confirming the HA formation in PDA-coated scaffolds.^{88–90} On the other hand, there are no visible HA characteristic peaks in gelatin-PEDOT:PSS constructs after the bioactivity test.

There is a possibility that the apatite mineralization mechanism of the PDA-coated scaffolds is due to an interaction between the negatively charged surface of the scaffolds and the ions of the SBF solution (Fig. 4G). Catecholamine functional groups (O–H and N–H₂) present in the PDA coating contribute to a negatively charged surface, due to their hydrophilic nature. Accordingly, Ca²⁺ ions can be adsorbed at the interface, and in consequence, PO₄^{3−} ions from SBF are attracted to the surface for finally nucleating calcium phosphate.⁹¹

3.8. Cell-scaffold interactions

In order to heal large bone defects, a stimulating framework must be provided for bone cells in the form of 3D structures (scaffolds). These scaffolds can be obtained off-the-shelf and serve as templates for bone growth. The effect of PDA coated constructs on cell adhesion was studied by seeding osteoblast-like MG-63 cells on gelatin-PEDOT:PSS scaffolds before and after PDA coating.

There was a significant relationship between the surface modification and the adhesion and spreading of cells. Fig. 5A and B represent the morphology after 2 days of MG-63 cells using FE-SEM images. It was evident that the cells covered the surface of both scaffold types by day 2. According to the FE-SEM micrographs, the cells formed filopodia in modified structures with PDA (Fig. 5B); however, the gelatin-PEDOT:PSS sample showed weaker cell adhesion and spreading (Fig. 5A).

Fig. 5C–H show the viability of the cells on PDA-coated and uncoated scaffolds. It is evident that MG-63 cells proliferate and are more evenly distributed on PDA-coated scaffolds (Fig. 5F–H) than on gelatin-PEDOT:PSS scaffolds (Fig. 5C–E). Therefore, cells cultured on coated constructs attached better, multiplied more, and had a higher viability than cells cultured on uncoated constructs. A study by Yang *et al.*⁹² demonstrated that mesenchymal stem cells cultured on poly(dimethylsiloxane) coated with PDA displayed greater adhesion and proliferation than on non-coated samples.

WST-8 assays were conducted at various time points (2, 4 and 7 days) to assess cell proliferation. In both scaffolds, more than 85 percent of cells were viable, indicating that the constructs are biocompatible and suitable for TE due to their non-significant toxic effects.¹⁰¹ The PDA coated scaffolds, however, have a higher density of viable cells after 2, 4 and 7 days of incubation than the gelatin-PEDOT:PSS scaffolds. In studies carried out by Steeves *et al.*⁹³ a positive influence of PDA on the proliferation of osteosarcoma cell lines (MG-63) has been confirmed. An enhancement in the density of live cells occurred for both uncoated and PDA coated samples over the course of the experiment, which may be related to nutrient-rich medium and lower stress (Fig. 5I). However, after day 4 of the WST-8 assay, a decrease is observed for both types of constructs. On the fourth day, constructs are expected to degrade, which may have led to the death of some cells due to the stress caused by



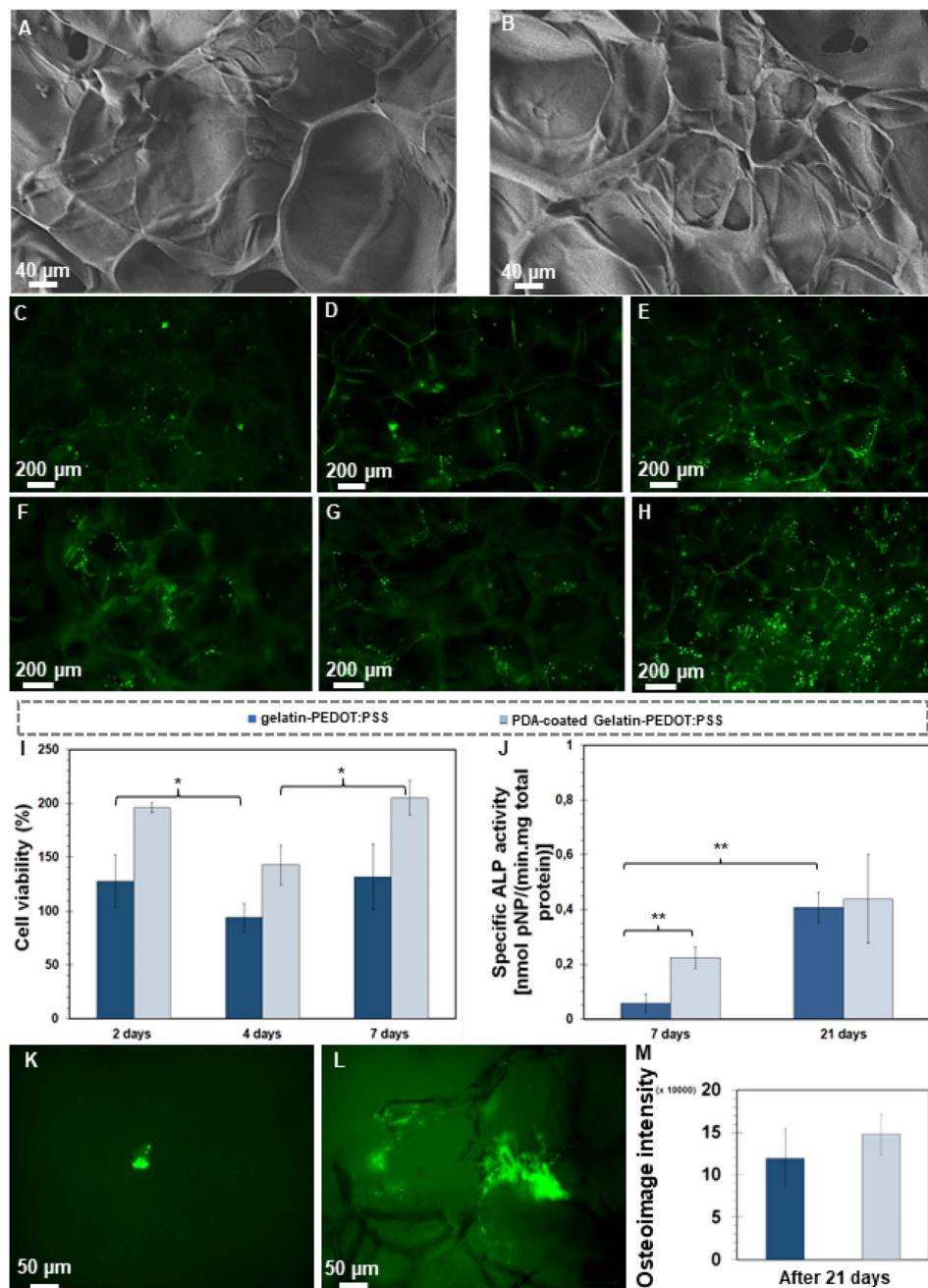


Fig. 5 Interaction of MG-63 cells with scaffolds. FE-SEM micrographs show cell morphology after 2 days of cell culture for (A) gelatin-PEDOT:PSS and (B) PDA coated gelatin-PEDOT:PSS scaffolds. (C–H) Cell viability via fluorescent microscopy images after calcein staining during (C, F) 2, (D, G) 4, and (E, H) 7 days (C–E) gelatin-PEDOT:PSS and (F–H) PDA coated gelatin-PEDOT:PSS. (I) WST-8 assay after 2, 4 and 7 days of culture in order to analyze cell proliferation. (J) ALP activity of polymeric scaffolds after 7 and 21 days culture. (K–M) Qualitative and quantitative osteoimage analysis to evaluate HA mineral deposition by the cells in modified and unmodified scaffolds. (Differences resulted statistically significant (* $p \leq 0.05$) and very statistically significant (** $p < 0.01$)).

degradation. In spite of this, cells were later capable to attach well to continue the proliferation process, leading to an increase in density of the cells within seven days.

MG-63 cells possess better attachment, spreading, and survival abilities when attached to PDA-coated gelatin-PEDOT:PSS scaffolds than when attached to unmodified scaffolds. Here, the interconnected pore structure of scaffolds also has a significant impact on the behavior of cells. It has been

found that scaffolds with both small and large pores provide a large surface area for cell attachment as well as influencing the movement of nutrients and fluids.⁹⁴ Gelatin contains arginyl-glycyl-aspartic acid (RGD) peptide sequences that are recognized by cell receptors.⁹⁵ They provide an abundance of adhesive motifs that promotes the anchoring and proliferation of implanted cells to the scaffolds, thereby improving cell affinity and tissue adhesiveness.^{96,97} Consequently, gelatin plays

a role in promoting cell proliferation and spreading.⁹⁸ Meanwhile, gelatin is well known for its hydrophilicity, which enables cells to adhere, proliferate, and migrate to the scaffold.⁹⁹ In addition, PEDOT:PSS itself has been found to contribute to cell viability, attachment, and proliferation in various previous studies^{61,100} due to its hydrophilicity and biocompatibility.

It has been shown that PDA coatings can facilitate the adhesion of peptides and nucleic acids as well as improve cell adhesion.^{100,101} Here, reaction with amine- or thiol-functionalized molecules of serum proteins provides active site for cell adhesion.¹⁰² Furthermore, PDA promotes endogenous fibronectin adsorption, which in turn enhances cell adhesion.¹⁰³ On the other hand, the study of Ge *et al.*,³⁰ indicated that PDA coating has a positive influence on the adhesion and growth of cells by providing surface roughness.

ALP is a secreted enzyme which indicates osteoblast differentiation, serving as a crucial parameter in assessing bone differentiation.¹⁰⁴ The activity of ALP is positively correlated with calcium deposition, biominerization, and osteogenic differentiation. After a successful adhesion and proliferation of cells, ALP will be expressed if cultured bioactive agents are available during the ECM maturation.¹⁰¹ According to Fig. 5J, MG-63 cells culturing on PDA coated and uncoated samples led to secretion of ALP at 7 and 21 days. PDA-coated gelatin PEDOT:PSS samples promoted five times higher ALP activity at day 7 than the control samples, indicating that the coated scaffolds are capable of stimulating bone formation at an early stage (statistically significant). In addition, the results demonstrate that for both modified and unmodified scaffolds, the ALP activity of MG-63 cells increases with time during the entire experimental period (21 days). PDA-containing scaffolds showed a 12.5% increase in ALP activity over uncoated samples after 21 days of culturing, which confirms their osteoinductive properties. Therefore, gelatin-PEDOT:PSS scaffolds coated with PDA are more likely to induce the maturation of osteoblast-like MG-63 cells than scaffolds without coatings.

Cell adhesion, growth, migration, and lineage specification have been shown to be influenced by matrix stiffness. Navarrete *et al.*¹⁰⁵ and Jiang *et al.*¹⁰⁶ demonstrated that more rigid matrices induce osteogenic differentiation of osteosarcoma cells by increasing the activity of the osteogenic marker ALP. Also, MG-63 cells are more likely to differentiate when exposed to PDA-coated samples. It was demonstrated that PDA supports the expression of ALP in human osteoblasts or mice osteoblasts as indicated in Kao *et al.*¹⁰⁷ and Zhang *et al.*¹⁰⁸ investigations, arising from the strong chelation effect of PDA that improves calcium ions level on the surface. Based on previous literature, PDA receptor-specific antagonists have been demonstrated to enhance angiogenesis by improving stem cell mobilization to wound sites,³⁶ while catechol moieties, amines, and hydroxyl functional groups in PDA interact with Ca^{2+} , thereby forming HA and creating an environment conducive to osteogenic proliferation and differentiation.

Mineralized nodules can be deposited by osteoblasts, resulting in complete mineralization of the bone matrix. OsteoImage™ Assay provides *in vitro* evidence of mineralization by staining the HA portion of bone-like nodules deposited by

cells with fluorescent OsteoImage™ Staining Reagent. Fig. 5K and L show the fluorescent microscope images taken by a fluorescent microscope after 21 days of cell culture. The formation of HA was observed after day 21 in gelatin-PEDOT:PSS scaffolds (Fig. 5K). However, large clusters of mineralization are visible in Fig. 5L corresponding to scaffolds that were coated with PDA. A quantitative evaluation of the OsteoImage test is also shown in Fig. 5M. The surface-modified constructs, however, are found to contain a greater amount of HA, supporting the qualitative results obtained previously. It has been demonstrated that the PDA-coated gelatin-PEDOT:PSS scaffolds are suitable for facilitating the differentiation of MG-63 cells and HA deposition that accelerates bone healing.

4. Conclusion

In this research, silane-modified gelatin-PEDOT:PSS scaffolds were fabricated using the freeze-drying technique, and functionalized with a PDA layer. The obtained electroconductive constructs showed a highly interconnected pore structure. Besides, a uniform and homogeneous PDA coating was successfully deposited on the surface of the constructs, which improved electrical and mechanical properties, water-scaffold interaction, and stability of scaffolds. Moreover, the bioactivity potential of the PDA-modified constructs after immersion in SBF suggests the possibility of their use as bone substitutes. The upgrade of properties after surface modification allowed the constructs to achieve MG-63 cell adhesion, proliferation, and osteogenic differentiation, as well as HA nodules precipitation. The formation of HA and osteogenic performance is recognized as a valuable and necessary criterion for assessing the bioactive potential of biomaterials; however, further research into the *in vivo* behavior of PDA-coated gelatin-PEDOT:PSS constructs is required before clinical evaluation. The effect of electrical conductivity on osteoblast cell behavior remains also a subject for future research.

Author contributions

Catalina Adler: methodology, investigation, data curation, visualization, writing – original draft. Mahshid Monavari: investigation, writing – original draft. Aldo R. Boccaccini, and Gustavo Abraham: conceptualization, writing – review & editing, supervision, project administration, funding acquisition. Farnaz Ghorbani: conceptualization, methodology, validation, visualization, writing – review & editing, supervision, project administration, funding acquisition.

Conflicts of interest

The authors whose names are listed certify that they have NO affiliations with or involvement in any organization or entity with any financial interest (such as honoraria; educational grants; participation in speakers' bureaus; membership, employment, consultancies, stock ownership, or other equity interest; and expert testimony or patent-licensing arrangements), or non-financial interest (such as personal or



professional relationships, affiliations, knowledge or beliefs) in the subject matter or materials discussed in this manuscript.

Acknowledgements

Catalina Adler thanks the IDEAR (Germany-Argentina Engineers) program (CUAA/DAHZ) for the scholarship to carry out an internship at FAU Erlangen-Nürnberg. Farnaz Ghorbani acknowledges the support of Alexander von Humboldt Foundation.

References

- 1 A. V. Boehm, S. Meininger, U. Gbureck and F. A. Müller, *Sci. Rep.*, 2020, **10**, 9430.
- 2 B. Thavornyutikarn, N. Chantarapanich, K. Sitthiseripratip, G. A. Thouas and Q. Chen, *Prog. Biomater.*, 2014, **3**, 61–102.
- 3 F. N. Alaribe, S. L. Manoto and S. C. K. M. Motaung, *Biologia*, 2016, **71**, 353–366.
- 4 M. Chimerad, A. Barazesh, M. Zandi, I. Zarkesh, A. Moghaddam, P. Borjian, R. Chimehrad, A. Asghari, Z. Akbarnejad, H. A. Khonakdar and Z. Bagher, *Int. J. Polym. Mater. Polym. Biomater.*, 2022, 1–25.
- 5 H. Shen and X. Hu, *RSC Adv.*, 2021, **11**, 6735–6747.
- 6 E. Capuana, F. Lopresti, F. Carfi Pavia, V. Brucato and V. La Carrubba, *Polymers*, 2021, **13**, 2041.
- 7 D. R. Katti, A. Sharma and K. S. Katti, in *Materials for Bone Disorders*, Elsevier, 2017, pp. 453–492.
- 8 C.-K. Kuo, H.-W. Huang, L.-G. Chen and Y.-J. Chou, *J. Asian Ceram. Soc.*, 2021, **9**, 1173–1182.
- 9 Y. D. Nokoorani, A. Shamloo, M. Bahadoran and H. Moravjei, *Sci. Rep.*, 2021, **11**, 16164.
- 10 J. Rnjak-Kovacina and A. S. Weiss, *Tissue Eng. Part B. Rev.*, 2011, **17**, 365–372.
- 11 M. J. Moore, E. Jabbari, E. L. Ritman, L. Lu, B. L. Currier, A. J. Windebank and M. J. Yaszemski, *J. Biomed. Mater. Res., Part A*, 2004, **71**, 258–267.
- 12 R. J. Mondschein, A. Kanitkar, C. B. Williams, S. S. Verbridge and T. E. Long, *Biomaterials*, 2017, **140**, 170–188.
- 13 N. Davari, N. Bakhtiary, M. Khajehmohammadi, S. Sarkari, H. Tolabi, F. Ghorbani and B. Ghalandari, *Polymers*, 2022, **14**, 986.
- 14 S. Kuttappan, D. Mathew and M. B. Nair, *Int. J. Biol. Macromol.*, 2016, **93**, 1390–1401.
- 15 M. Nouri-Felekori, A. S. M. Mesgar and Z. Mohammadi, *Ceram. Int.*, 2015, **41**, 6013–6019.
- 16 S. Farris, J. Song and Q. Huang, Alternative Reaction Mechanism for the Cross-Linking of Gelatin with Glutaraldehyde, *J. Agric. Food Chem.*, 2010, **58**(2), 998–1003.
- 17 F. Ghorbani, A. Zamanian, A. Behnamghader and M. D. M. D. Joupari, *Mater. Sci. Eng. C*, 2019, **94**, 729–739.
- 18 L. Sun, S. Li, K. Yang, J. Wang, Z. Li and N. Dan, *J. Leather Sci. Eng.*, 2022, **4**, 1.
- 19 F. Ghorbani, A. Zamanian, A. Behnamghader and M. Daliri Joupari, *J. Appl. Polym. Sci.*, 2018, **135**, 46739.
- 20 J. Manissorn, P. Wattanachai, K. Tonsomboon, P. Bumroongsakulsawat, S. Damrongsakkul and P. Thongnuek, *Mater. Today Commun.*, 2021, **26**, 101730.
- 21 H. Derakhshankhah, M. Eskandani, S. Akbari Nakhjavani, S. Tasoglu, S. Vandghanooni and M. Jaymand, *Int. J. Polym. Mater. Polym. Biomater.*, 2023, 1–13.
- 22 H. Nekounam, H. Samadian, S. Bonakdar, F. Asghari, M. A. Shokrgozar and R. F. Majidi, *Life Sci.*, 2021, **282**, 119602.
- 23 Z. E. Dibazar, M. Mohammadpour, H. Samadian, S. Zare, M. Azizi, M. Hamidi, R. Elbouthachfai, E. Petit and C. Delattre, *Mater.*, 2022, **15**, 2494.
- 24 S. Ghaziof, S. Shojaei, M. Mehdikhani, M. Khodaei and M. Jafari Nodoushan, *J. Mech. Behav. Biomed. Mater.*, 2022, **132**, 105271.
- 25 F. Heidari, M. E. Bahrololoom, D. Vashaei and L. Tayebi, *Ceram. Int.*, 2015, **41**, 3094–3100.
- 26 B. C. Heng, Y. Bai, X. Li, Y. Meng, Y. Lu, X. Zhang and X. Deng, *Anim. Model. Exp. Med.*, 2023, 1–11.
- 27 R. Lay, G. S. Deijs and J. Malmström, *RSC Adv.*, 2021, **11**, 30657–30673.
- 28 R. Arambula-Maldonado and K. Mequanint, *Mater. Adv.*, 2022, **3**, 5186–5206.
- 29 M. A. Marsudi, R. T. Ariski, A. Wibowo, G. Cooper, A. Barlian, R. Rachmantyo and P. J. D. S. Bartolo, *Int. J. Mol. Sci.*, 2021, **22**, 11543.
- 30 L. Ge, Q. Li, Y. Huang, S. Yang, J. Ouyang, S. Bu, W. Zhong, Z. Liu and M. MQ Xing, *J. Mater. Chem. B*, 2014, **40**, 6917.
- 31 F. J. Chen, Y. S. Hsiao, I. H. Liao, C. T. Liu, P. I. Wu, C. Y. Lin, N. C. Cheng and J. Yu, *J. Mater. Chem. B*, 2021, **9**, 7674–7685.
- 32 A. G. Guex, J. L. Puetzer, A. Armgarth, E. Littmann, E. Stavrinidou, E. P. Giannelis, G. G. Malliaras and M. M. Stevens, *Acta Biomater.*, 2017, **62**, 91–101.
- 33 M. S. Kang, S. J. Jeong, S. H. Lee, B. Kim, S. W. Hong, J. H. Lee and D.-W. Han, *Biomater. Res.*, 2021, **25**, 4.
- 34 P. Dharmalingam, G. Palani, R. Apsari, K. Kannan, S. K. Lakkaboyana, K. Venkateswarlu, V. Kumar and Y. Ali, *Mater. Today Sustain.*, 2022, **20**, 100232.
- 35 T. Ghassemi, A. Shahroodi, M. H. Ebrahimzadeh, A. Mousavian, J. Movaffagh and A. Moradi, *Arch. Bone Jt. Surg.*, 2018, **6**, 90.
- 36 F. Ghorbani, A. Zamanian and M. Sahranavard, *Biomed. Eng./Biomed. Tech.*, 2019, **65**, 273–287.
- 37 J. Fernández, O. Auzmendi, H. Amestoy, A. Diez-Torre and J. R. Sarasua, *Eur. Polym. J.*, 2017, **94**, 208–221.
- 38 B. Ghalandari, Y. Yu, F. Ghorbani, A. R. Warden, K. Z. Ahmad, X. Sang, S. Huang, Y. Zhang, W. Su, A. Divsalar and X. Ding, *Nanoscale*, 2021, **13**, 20098–20110.
- 39 N. Kaushik, L. N. Nguyen, J. H. Kim, E. H. Choi and N. K. Kaushik, *Int. J. Mol. Sci.*, 2020, **21**, 1–19.
- 40 X. Chen, L. Zhu, H. Liu, W. Wen, H. Li, C. Zhou and B. Luo, *Biomed. Mater.*, 2019, **14**, 055005.
- 41 N. Analytech, *Resistivity measuring systems: Resistance and Resistivity*, <https://www.nh-instruments.de/en/>.
- 42 A. Montes, D. Valor, L. Delgado, C. Pereyra and E. Martínez de la Ossa, *Polymers*, 2022, **14**, 488.



43 T. Kokubo and H. Takadama, *Biomaterials*, 2006, **27**, 2907–2915.

44 W. Zhuang, G. Ye, J. Wu, L. Wang, G. Fang, Z. Ye, G. Lai, X. Qiu and H. Sang, *Biomater. Adv.*, 2022, **133**, 112619.

45 Z. Xu, N. Wang, P. Liu, Y. Sun, Y. Wang, F. Fei, S. Zhang, J. Zheng and B. Han, *Molecules*, 2019, **24**, 4397.

46 L. Han, Y. Jiang, C. Lv, D. Gan, K. Wang, X. Ge and X. Lu, *Colloids Surf. B Biointerfaces*, 2019, **179**, 470–478.

47 S. Kasemset, L. Wang, Z. He, D. J. Miller, A. Kirschner, B. D. Freeman and M. M. Sharma, *J. Membr. Sci.*, 2017, **522**, 100–115.

48 C. Murphy, M. Haugh and F. O'Brien, *Biomaterials*, 2010, **31**, 461–466.

49 N. Abbasi, S. Hamlet, R. M. Love and N. T. Nguyen, *J. Sci. Adv. Mater. Devices*, 2020, **5**, 1–9.

50 C. Shen, J. Liu, Q. Lu, G. Wang, Z. Wang and L. Liu, *Int. J. Nanomedicine*, 2022, **17**, 681.

51 M. Di Foggia, P. Taddei, A. Torreggiani, M. Dettin and A. Tinti, *Proteomics Res. J.*, 2011, **2**, 231.

52 C. Tonda-Turo, P. Gentile, S. Saracino, V. Chiono, V. K. Nandagiri, G. Muzio, R. A. Canuto and G. Ciardelli, *Int. J. Biol. Macromol.*, 2011, **49**, 700–706.

53 D. Choi, M. Qiu, Y.-C. Hwang, W.-M. Oh, J.-T. Koh, C. Park and B.-N. Lee, *Materials*, 2022, **15**, 2170.

54 C. E. Campiglio, N. Contessi Negrini, S. Farè and L. Draghi, *Materials*, 2019, **12**, 2476.

55 F. Ghorbani, A. Zamanian, A. Behnamghader and M. Daliri Joupari, *Mater. Sci. Eng. C*, 2020, **112**, 110906.

56 H. C. Chang, T. Sun, N. Sultana, M. M. Lim, T. H. Khan and A. F. Ismail, *Mater. Sci. Eng. C*, 2016, **61**, 396–410.

57 S. Xiong, L. Zhang and X. Lu, *Polym. Bull.*, 2013, **70**, 237–247.

58 G. M. Nazmul Islam, M. Azam Ali and S. Collie, *Fibers Polym.*, 2022, **23**, 914–924.

59 X. Hu, Y. Ke, M. Zhang, H. Niu, D. Wu and L. Zhao, *High Perform. Polym.*, 2021, **33**, 601–614.

60 F. Ghorbani, A. Zamanian, A. Behnamghader and M. Daliri Joupari, *Surface. Interfac.*, 2019, **15**, 38–42.

61 N. Fani, M. Hajinasrollah, M. H. Asghari Vostikolaee, M. Baghaban Eslaminejad, F. Mashhadiabbas, N. Tongas, M. Rasoulianboroujeni, A. Yadegari, K. F. Ede, M. Tahriri and L. Tayebi, *J. Bioact. Compat. Polym.*, 2019, **34**, 436–441.

62 W. W. Hu, T. C. Chen, C. W. Tsao and Y. C. Cheng, *J. Biomed. Mater. Res. B Appl. Biomater.*, 2019, **107**, 1607–1619.

63 R. A. Gittens, R. Olivares-Navarrete, R. Rettew, R. J. Butera, F. M. Alamgir, B. D. Boyan and Z. Schwartz, *Bioelectromagnetics*, 2013, **34**, 599–612.

64 A. Shahini, M. Yazdimamaghani, K. J. Walker, M. A. Eastman, H. Hatami-Marbini, B. J. Smith, J. L. Ricci, S. V. Madihally, D. Vashaee and L. Tayebi, *Int. J. Nanomedicine*, 2014, **9**, 167.

65 J. Gopinathan, M. M. Pillai, K. S. Sahanand, B. K. D. Rai, R. Selvakumar and A. Bhattacharyya, *Biomed. Mater.*, 2017, **12**, 065001.

66 N. Shadjou, M. Hasanzadeh and B. Khalilzadeh, *Bioengineered*, 2018, **9**, 38–47.

67 C. Xie, P. Li, L. Han, Z. Wang, T. Zhou, W. Deng, K. Wang and X. Lu, *NPG Asia Mater.*, 2017, **9**, e358.

68 Y. Liu, K. Ai and L. Lu, *Chem. Rev.*, 2014, **114**, 5057–5115.

69 J. Shen, D. Shi, L. Dong, Z. Zhang, X. Li and M. Chen, *J. Biomed. Mater. Res., Part A*, 2018, **106**, 3255–3266.

70 E. Ryan and S. Yin, *Ceram. Int.*, 2022, **48**, 15516–15524.

71 H. Lee, J. Rho and P. B. Messersmith, *Adv. Mater.*, 2009, **21**, 431–434.

72 T. N. Dinh, S. Hou, S. Park, B. A. Shalek and K. J. Jeong, *ACS Biomater. Sci. Eng.*, 2018, **4**, 3471–3477.

73 S. H. Ku and C. B. Park, *Biomaterials*, 2010, **31**, 9431–9437.

74 J. Shen, D. Shi, L. Dong, Z. Zhang, X. Li and M. Chen, *J. Biomed. Mater. Res., Part A*, 2018, **106**, 3255–3266.

75 S. A. Chinchulkar, P. Patra, D. Dehariya, A. Yu and A. K. Rengan, *Polym. Adv. Technol.*, 2022, **33**, 3935–3956.

76 R. Marsell and T. A. Einhorn, *Injury*, 2011, **42**, 551–555.

77 M. Nouri-Felekori, M. Khakbiz, N. Nezafati, J. Mohammadi and M. B. Eslaminejad, *Int. J. Pharm.*, 2019, **557**, 208–220.

78 D. A. Ahmad Ruzaidi, M. M. Mahat, S. A. Shafee, Z. Mohamed Sofian, A. S. Mohmad Sabere, R. Ramlie, H. Osman, H. H. Hamzah, Z. Zainal Ariffin and K. K. Sadasivuni, *Polymers*, 2021, **13**, 3395.

79 F. Ghorbani, M. Kim, M. Monavari, B. Ghalandari and A. R. Boccaccini, *Front. Bioeng. Biotechnol.*, 2022, **10**, 940070.

80 D. Vona, S. R. Cicco, R. Ragni, C. Vicente-Garcia, G. Leone, M. M. Giangregorio, F. Palumbo, E. Altamura and G. M. Farinola, *Photochem. Photobiol. Sci.*, 2022, **21**, 949–958.

81 J. R. Jones, L. M. Ehrenfried and L. L. Hench, *Biomaterials*, 2006, **27**, 964–973.

82 N. Mamat, M. Jaafar, Z. A. A. Hamid and B. H. Yahaya, *J. Phys. Conf.*, 2019, **1372**, 012054.

83 P. Feng, X. Qiu, L. Yang, Q. Liu, C. Zhou, Y. Hu and C. Shuai, *Colloids Surf. B Biointerfaces*, 2022, **217**, 112668.

84 S. Dimassi, N. Tabary, F. Chai, C. Zobrist, J. C. Hornez, F. Cazaux, N. Blanchemain and B. Martel, *Carbohydr. Polym.*, 2022, **276**, 118774.

85 Z. I. Dhary, A. A. Atiyah and S. B. H. Farid, 2022, vol. **2450**, p. 020011.

86 P. Madani, *Adv. Ceram. Prog.*, 2022, **8**, 18–26.

87 T. Sirisoam, C. Saelee, S. Thiansem and S. Punyanitya, *Mater. Sci. Forum*, 2018, **940**, 3–7.

88 Z. Tabia, S. Akhtach, K. El Mabrouk, M. Bricha, K. Nouneh and A. Ballamurugan, *Biomed. Glas.*, 2020, **6**, 10–22.

89 T. H. Dang, T. H. Bui, E. V. Guseva, A. T. Ta, A. T. Nguyen, T. T. H. Hoang and X. V. Bui, *Crystals*, 2020, **10**, 1–10.

90 Q. Qiu, X. Ding, Y. Wang, Y. Zheng, L. Zhu, Y. Li and T. Liu, *Mater. Today Commun.*, 2022, **32**, 104098.

91 P. Feng, M. Liu, S. Peng, S. Bin, Z. Zhao and C. Shuai, *J. Mater. Res. Technol.*, 2021, **15**, 3375–3385.

92 D. H. Yang, S. Jung, J. Y. Kim and N. Y. Lee, *Micromachines*, 2022, **13**, 1122.

93 A. J. Steeves, A. Atwal, S. C. Schock and F. Variola, *J. Mater. Chem. B*, 2016, **4**, 3145–3156.

94 C. M. Murphy and F. J. O'Brien, *Cell Adh. Migr.*, 2010, **4**, 377–381.



95 O. Jeznach, D. Kołbuk, T. Reich and P. Sajkiewicz, *Polymers*, 2022, **14**, 4154.

96 L. Yan, T. Zhou, R. Ni, Z. Jia, Y. Jiang, T. Guo, K. Wang, X. Chen, L. Han and X. Lu, *ACS Appl. Bio Mater.*, 2022, **5**, 4366–4377.

97 F. Fayyabakhsh, M. J. Khayat and M. C. Leu, *Int. J. Bioprinting*, 2022, **8**, 618.

98 C. Liu, Q. Yu, Z. Yuan, Q. Guo, X. Liao, F. Han, T. Feng, G. Liu, R. Zhao, Z. Zhu, H. Mao, C. Zhu and B. Li, *Bioact. Mater.*, 2023, **25**, 445–459.

99 A. Karakeçili, S. Korpayev and K. Orhan, *Appl. Biochem. Biotechnol.*, 2022, **194**, 3843–3859.

100 C.-C. Lin and S.-J. Fu, *Mater. Sci. Eng. C*, 2016, **58**, 254–263.

101 F. Ghorbani, B. Ghalandari, A. L. Khan, D. Li, A. Zamanian and B. Yu, *Biotechnol. Prog.*, 2020, **36**, e3043.

102 I. Singh, G. Dhawan, S. Gupta and P. Kumar, *Front. Microbiol.*, 2021, **11**, 607099.

103 Y. H. Ding, M. Floren and W. Tan, *Biosurf. Biotribol.*, 2016, **2**, 121–136.

104 S. L. Moura, A. Pallarès-Rusíñol, L. Sappia, M. Martí and M. I. Pividori, *Biosens. Bioelectron.*, 2022, **198**, 113826.

105 R. Olivares-Navarrete, E. M. Lee, K. Smith, S. L. Hyzy, M. Doroudi, J. K. Williams, K. Gall, B. D. Boyan and Z. Schwartz, *PLoS One*, 2017, **12**, e0170312.

106 T. Jiang, J. Zhao, S. Yu, Z. Mao, C. Gao, Y. Zhu, C. Mao and L. Zheng, *Biomaterials*, 2019, **188**, 130–143.

107 C.-T. Kao, C.-C. Lin, Y.-W. Chen, C.-H. Yeh, H.-Y. Fang and M.-Y. Shie, *Mater. Sci. Eng. C*, 2015, **56**, 165–173.

108 J. Zhang, J. Li, G. Jia, Y. Jiang, Q. Liu, X. Yang and S. Pan, *RSC Adv.*, 2017, **7**, 56732–56742.

